Fibers Discriminant

by Lina Septiana

Submission date: 09-Sep-2022 10:57AM (UTC+0700)
Submission ID: 1895637911
File name: File220823221409220823221409050318098401.pdf (4.7M)
Word count: 3830
Character count: 21525

cal Review (2019) 26:369–379
https://doi.org/10.1007/s10043-019-00512-8

REGULAR PAPER

Elastic and collagen fibers discriminant analysis using H&E stained hyperspectral images

Lina Septiana[1,5] · Hiroyuki Suzuki[2] · Masahiro Ishikawa[3] · Takashi Obi[1,2] · Naoki Kobayashi[3] · Nagaaki Ohyama[2] · Takaya Ichimura[4] · Atsushi Sasaki[4] · Erning Wihardjo[5] · Dini Andiani[6]

Received: 17 December 2018 / Accepted: 21 May 2019 / Published online: 31 May 2019

Abstract

Hematoxylin and eosin (H&E) stain is one of the most common specimen staining methods in pathology diagnosis due to the capability to show the morphological structure of tissue. However, the appearance of the specific component, i.e., elastic fibers might not be recognized easily because have similar color and pattern with ones of collagen fibers. To distinguish these two components, Verhoeff's Van Gieson (EVG) staining method is commonly used. Nevertheless, procedures of EVG stain are more complex and expensive than H&E stain. In this study, we investigate the possibility to distinguish elastic and collagen fibers from H&E stained images by applying spectral image analysis based on hyperspectral images. With experiments, we measure the transmittance spectral of 61-band H&E stained hyperspectral image, which are converted into absorbance spectral of hematoxylin, eosin, and red blood cell. As many as 3000 sampling pixels both from RGB and hyperspectral images of HE stained specimens were trained using Linear Discriminant Analysis (LDA) to get a discriminant function to classify elastic and collagen components in H&E RGB and H&E hyperspectral images. We conducted verification based on leave-one-out cross-validation of six data sets for evaluation. The verification result both visually and quantitatively compared to EVG stained image shows that the usage of hyperspectral images performs better than RGB images.

Keywords Pathology · Hyperspectral image · Discriminant analysis · Classification

1 Introduction

In recent clinical practice, image-based diagnostic technologies become increasingly important. Accordingly, there is a demand for improvement of techniques for analyzing complex biological tissues. Despite recently radiological imaging systems are progressively developed, the evaluation of tissues by biopsy and clinical pathology examination remains the gold standard for definite diagnosis.

In pathology diagnosis, specimen staining is an important process, in which the color information obtained by tissue components is useful for further pathological analysis. Hematoxylin and eosin (H&E) stain, which is one of the most common staining methods, is conducted in almost all pathological diagnosis to observe the morphological structures of tissues. In H&E stained images, fibers and cytoplasm are stained pink and nuclei are stained blue. On the other hand, previous studies about pathological analysis showed obvious correlation between the abnormality of elastic fibers and diseases [1]. Specifically, it is well known that pancreatic cancer tissues have a specific

✉ Lina Septiana
septiana.l.aa@m.titech.ac.jp

1 Department of Information and Communication Engineering, School of Engineering, Tokyo Institute of Technology, Yokohama, Kanagawa 226-8503, Japan
2 Institute of Innovative Research, Tokyo Institute of Technology, Yokohama, Kanagawa 226-8503, Japan
3 Faculty of Health and Medical Care, Saitama Medical University, Iruma, Saitama 350-0495, Japan
4 Faculty of Medicine, Saitama Medical University, Iruma, Saitama 350-0495, Japan
5 Department of Electrical Engineering, Krida Wacana Christian University, Jakarta 11470, Indonesia
6 Research Center for Quality System and Testing Technology, Indonesian Institute of Sciences (P2SMTP-LIPI), Tangerang 15310, Indonesia

density and distribution of elastic fibers in the walls of vessels and ducts associated with the tumor phenomenon in pancreatic ductal carcinoma [2]. However, the appearance of elastic fibers is not easy to be recognized from H&E stained images, due to the similar color and pattern with collagen fibers. To distinguish these two components, Verhoeff's Van Gieson (EVG) stained images are commonly used because EVG stain is able to dye elastic and collagen fibers different colors, deep blue and orchid, respectively. Nevertheless, procedures of EVG stain are more complicated and less cost-efficient than H&E stain.

Meanwhile, hyperspectral imaging techniques have been studied for a long time in various applications such as remote sensing [3], and recently it has been extended to the pathology field [4]. Using hyperspectral microscopic cameras, tissue specimens can be analyzed in more narrow and various wavelength bands than using general RGB cameras. Due to this technique, we can obtain valuable and comprehensive information regarding the object characteristic on biomedical tissues [4–7]. If this technique is employed to analyze H&E stained images, elastic and collagen fibers may be able to be classified without EVG stained images. This means that we can reduce the time consumption and cost. Therefore, we investigate the possibility to distinguish elastic and collagen fibers without EVG stained specimens but with H&E stained ones by applying spectral image analysis based on hyperspectral images. As a target to confirm the efficiency of hyperspectral image analysis, we examine pancreas tissue samples.

2 Material and method

Procedures in this study consist of several steps, i.e., image acquisition, preprocessing, training, dimensional reduction, classification, and verification. More detailed procedures can be seen in the block diagram shown in Fig. 1.

2.1 Image acquisition

2.1.1 Tissue samples

Motivated by previous research that the specific appearance of elastic fibers is a tumor-associated phenomenon in pancreatic ductal carcinoma [2], hence human pancreas in H&E stained and EVG stained tissue specimens from BioMax Inc. are used in this experiment. All tissues are collected under the highest ethical standards with the donor being informed completely and with their consent.

We used six pairs of tissue sample images, each pair consists of an H&E stained specimen and an EVG stained one, which have almost exactly same biological structures. That is because these EVG stained specimens are obtained by dying unstained specimens that are obtained by bleaching the H&E stained specimens. H&E stained specimens as

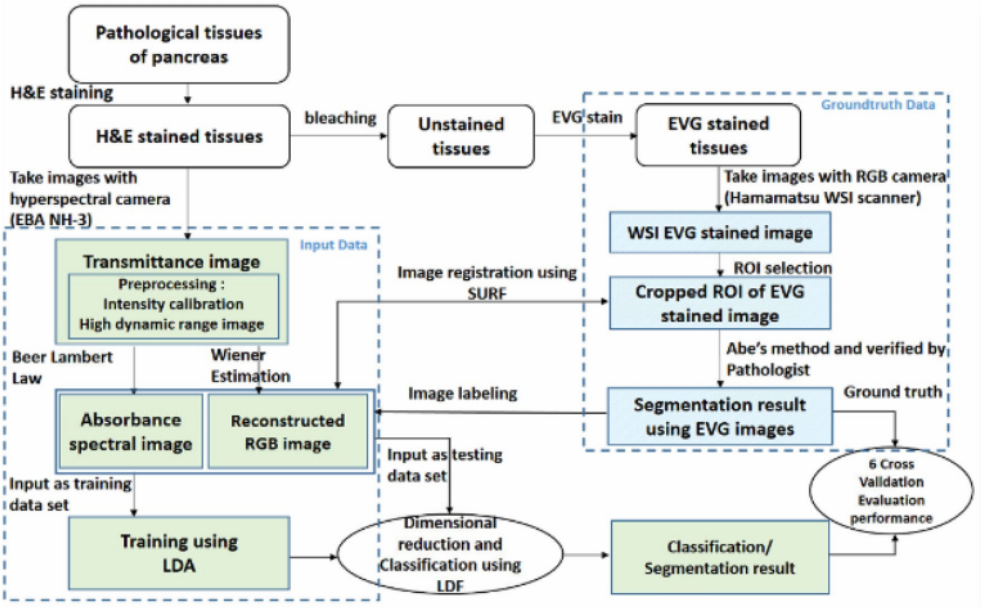

Fig. 1 Block diagram of procedures

shown in Fig. 2a are captured with a hyperspectral camera that is attached to a microscope. In this case, we select smaller region of interest (ROI)s manually from the sample tissue as shown in Fig. 2c. They are used for classification of elastic and collagen fibers. EVG stained images are captured with a whole slide image (WSI) scanner by Hamamatsu photonics K.K. They are used for evaluation of the experiment, i.e., the classification results from the EVG stained images help us to find groundtruth.

2.1.2 Hyperspectral imaging system

Hyperspectral images are captured with a hyperspectral camera, NH-3 by EBA JAPAN CO., Ltd. It can take 151 band images from 350 to 1100 nm with 5 nm wavelength resolution interval. We only used 61 visible wavelengths from 420 to 720 nm. The image size is 752×480 pixels, and the data length on each pixel is 10 bits with intensity range 0–4095 (interval value 4) which is equal to 12 bits. Tissue samples are observed with an optical microscope, BX-53 by Olympus Corp., with which the hyperspectral camera and a white LED light source are attached. The above hyperspectral imaging system is based on transmission measurement, and hence a calibrated transmittance image $t(\lambda)$ is obtained as following equation [8],

$$t_i(\lambda) = \frac{I(\lambda)_s/E_s - I(\lambda)_{bl}/E_{bl}}{I(\lambda)_w/E_w - I(\lambda)_{bl}/E_{bl}}, \quad (1)$$

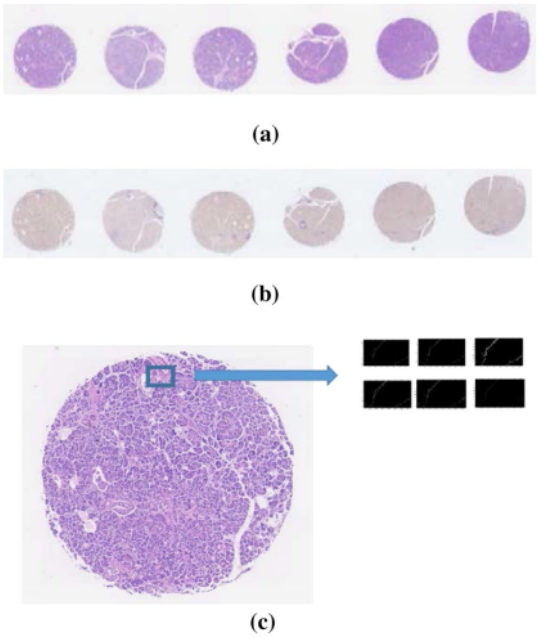

Fig. 2 Pancreas tissues specimen **a** H&E stained image, **b** EVG stained image, **c** ROI images of hyperspectral image

where $I(\lambda)_{bl}$ is a black image pixel with LED off, $I(\lambda)_w$ is a white image pixel which goes through an empty glass slide with LED on, $I(\lambda)_s$ is a captured sample image pixel, E_s is an exposure of the captured sample image $I(\lambda)_s$, E_{bl} is an exposure of the black image $I(\lambda)_{bl}$, and E_w is a total exposure of the white image $I(\lambda)_w$.

To avoid any structural information loss within saturated regions, we employ a high-dynamic-range rendering technique, i.e., we take both of high and low exposure images, and the saturated areas in the high exposure image are replaced with the values come from the low exposure image.

To make the object of interest in tissue easier to be analyzed, we calculate the absorbance image intensity using Beer Lambert Law [8–10] as follows,

$$\text{Absorbance image}\,(\lambda) = -\log_{10}\{t(\lambda)\}. \quad (2)$$

2.2 Linear discriminant analysis (LDA)

The absorbance spectra derived from the hyperspectral images are explored for any observable phenomena such as pixel clusters of elastic and collagen fibers. For this purpose, we use linear discriminant analysis (LDA), a multivariate statistical analysis method for dimensionality reduction and for classification based on the largest possible variance. The reason why we use LDA is because we can directly observe the potential of the measured data itself to classify elastic and collagen fibers, without dependence on skills and experience as a data scientist. On the other hand, the performance of sophisticated classification methods such as deep learning is much more dependent on skills and experience, although the accuracy might be better than LDA, i.e., sophisticated methods might have a negative influence for fair evaluation.

The computation step of LDA as follows [11, 12].

We calculate mean vectors of image intensities in elastic and collagen fiber regions as follows,

$$\mu_1 = \sum_{i=1}^{n_1} x_{1i}/n_1, \quad \mu_2 = \sum_{i=1}^{n_2} x_{2i}/n_2, \quad (3)$$

where μ_1 is a mean vector of image intensities in elastic fibers, μ_2 is a mean vector of image intensities in collagen fibers, x_{1i} is an image intensity of an elastic fiber region from ith pixel sample, x_{2i} is an image intensity of collagen fiber regions from ith pixel sample, n_1 is a number of pixels in elastic fibers, and n_2 is a number of pixels in collagen regions.

Then, we calculate within-class scatter matrix W as follows,

$$W = n_1 \times \sum_{x_{1i} \in \text{Elastic}} (x_{1i} - \mu_1)(x_{1i} - \mu_1)^t + n_2 \times \sum_{x_{2i} \in \text{Collagen}} (x_{2i} - \mu_2)(x_{2i} - \mu_2)^t. \quad (4)$$

Between-class scatter matrix can be defined by sample covariance of the class mean,

$$B = \sum_{i=1}^{2} n_i (\mu_i - \mu)(\mu_i - \mu)^t, \tag{5}$$

where μ is a mean vector of both elastic and collagen fibers.

The jth classification vector $\vec{v_j}$ in this case will be given by,

$$B\vec{v_j} = \lambda W\vec{v_j}. \tag{6}$$

Then, we can obtain the classification vector $\vec{v_j}$ by calculating an eigenvector of $\mathrm{W}^{-1}B$.

This study uses the first eigenvector of LDA as a linear discriminant function (LDF) for classification of Elastin and Collagen. An inner product between the LDF and a spectrum on a pixel of an H&E stained hyperspectral image is calculated as a score for classification.

3 Experiments results

3.1 Training data of H&E stained image

For training data, we picked 3000 pixel samples including 1500 elastic and 1500 collagen fibers from 6 H&E stained tissue samples. The positions of the sampled points were selected by non-pathologist based on the label from groundtruth EVG stained images produced by using Abe's method which has been revised according to pathologists' suggestion. The EVG images were exactly aligned and scale-adjusted with the corresponding H&E-stained images by employing an image registration technique based on speeded-up robust features (SURF). Hence, we could identify the correct positions of the elastic and collagen fiber samples in the H&E-stained images.

Figure 3 shows pixel values of all training data samples in H&E-stained images. In Fig. 3a, red plots represent collagen fibers, and blue plots represent elastic fibers in RGB images. Figure 3b shows the measured intensity values of hyperspectral images as 61 bands. Using these samples, we conducted LDA and obtained an LDF for the classification of elastic and collagen fibers in H&E-stained images. Figure 4a shows the eigenvalues of the matrix $W^{-1}B$ in Eq. (6). This graph means that the first classification vector generated by LDA makes a much larger contribution to the classification performance than others. That is why we use only the first classification vector as LDF. Figure 4b shows the LDF for hyperspectral image and also the LDF for RGB image is obtained as following vector,

$$\mathrm{LDF_{RGB}} = \begin{pmatrix} -0.6428 \\ 0.6538 \\ 0.3991 \end{pmatrix}, \tag{7}$$

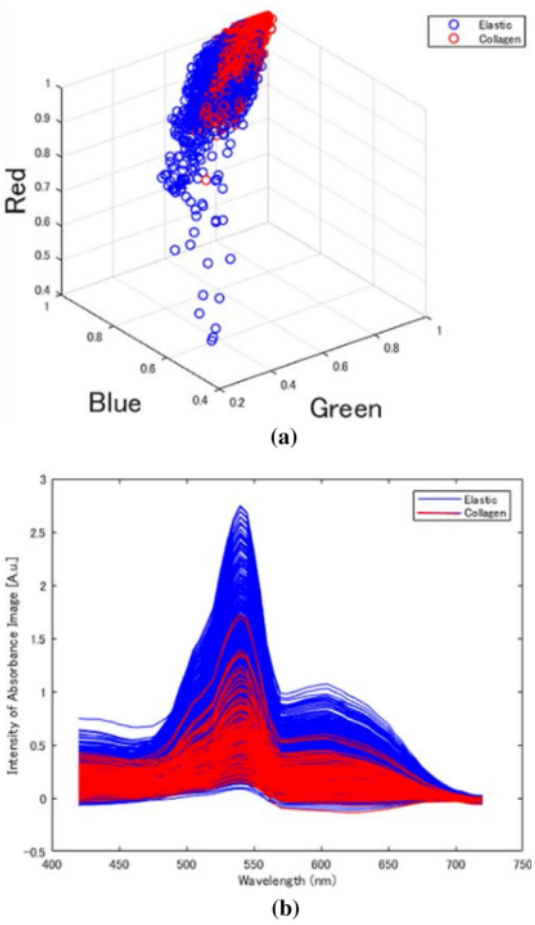

Fig. 3 Pixel values of training data samples in H&E stained image. **a** RGB image, **b** hyperspectral image

where each component of this vector shows LDF coefficients for R, G, and B, respectively.

3.2 Classification result

To classify the regions of elastic and collagen fibers from H&E stained images, we applied the LDFs as shown in Fig. 4 and Eq. (7) to H&E stained RGB and hyperspectral testing images. We conducted additional experiments based on 6 Leave-one-out cross-validations, which consist of five image samples for training and the other 1 image sample for testing and repeat validations for all 6 sets of image samples. In each cross-validation, 600 pixels which consist of 300 pixels in elastic fiber regions and 300 pixels in collagen ones were taken from each image sample.

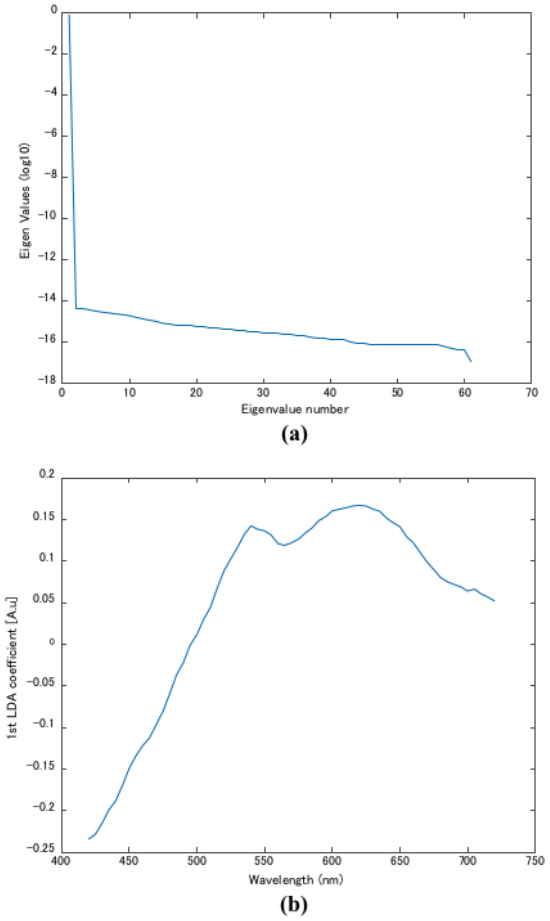

Fig. 4 Example result of LDA for training dataset **a** Eigen values, **b** LDF for classification of elastic and collagen fibers in hyperspectral images

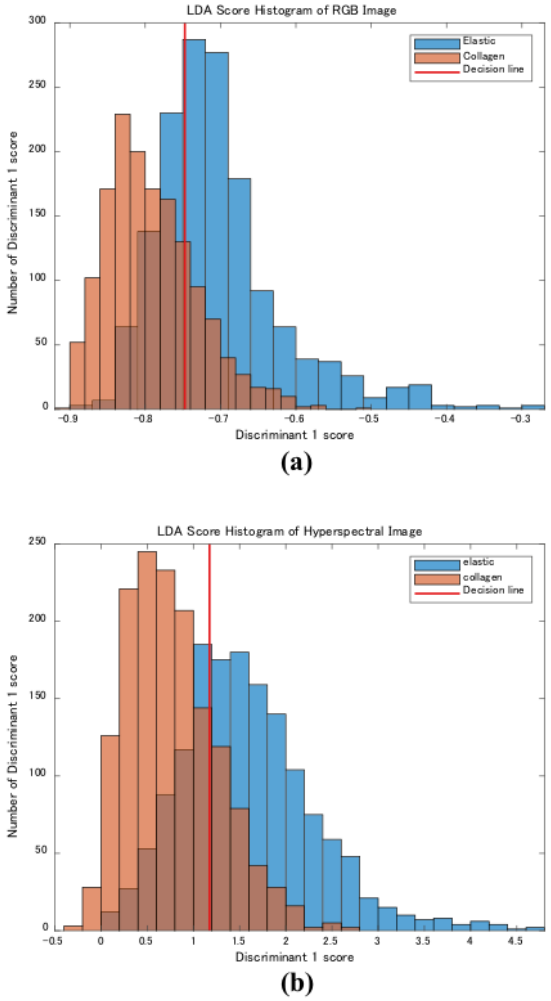

Fig. 5 Distributions of LDF data projections **a** RGB image, **b** hyperspectral image

As a pre-processing, we extracted only fiber regions from the H&E stained images. The procedures of this pre-processing was as follows;

1. Fiber regions of EVG stained images are extracted by employing Abe's method for EVG image [13]. The extracted regions have been verified by pathologists from Saitama Medical University, and the collagen and elastic fiber regions as groundtruth images have been revised according pathologists' suggestion.
2. Fiber regions of H&E stained images are extracted by tracing the extracted region of the EVG stained images, which are exactly aligned and scale-adjusted with the corresponding H&E stained images by employing the SURF-based image registration.

The reason why we did this procedure is that this study did not consider the classification of all pathology elements but only focused on the potential classification of elastic and collagen fibers in H&E stained specimens based on spectral information only.

For evaluation, we examined distributions of LDF data projections using test samples. We calculated data projections between the LDFs and pixel values of fiber regions in the test samples and used the data projections as scores for classification. Figure 5a, b show histograms of the data projection for RGB and hyperspectral images, respectively. We can see that the distributions of elastic and collagen fibers in the hyperspectral images are separated more significantly than the RGB images. In addition,

we calculated decision lines for optimal classification, which are represented as red lines in Fig. 5. The decision lines are expected to reach the condition where the error rate of the classification is minimum and equal for two classes [14–16]. When the score is larger than the decision line, its sample pixel is decided as elastic fiber, while it is decided as collagen fiber in the opposite case. Figure 6 shows six pairs of H&E and EVG image samples for cross-validation, and Fig. 7 shows resultant images of classification from one cross-validation. Figure 7a–e show extracted fiber regions of an H&E-stained image, a classification resultant image from an RGB H&E stained image, a classification resultant image from a hyperspectral H&E image, extracted fiber regions of an EVG stained image, and a groundtruth image produced from an EVG image, respectively.

In Fig. 7b, c, e, red color pixels on these images indicate the appearance of collagen fiber, and blue color pixels also indicate elastic fibers, and white squares in each image show the characteristic regions, in which a large square exhibits zoomed part of a small square area. Figure 8 also shows resultant images for all six cross-validations. Figure 8a–c show groundtruth images, resultant images from hyperspectral H&E images, and resultant images from RGB H&E images, respectively. From these resultant images, we can see that the resultant images of elastic and collagen fiber classification using hyperspectral images shaped more similar pattern to the groundtruth image than using RGB images.

Beside visual verification, we also calculated the sensitivity and specificity, which are quantitative evaluation indexes for classification. They are defined as following equations [17],

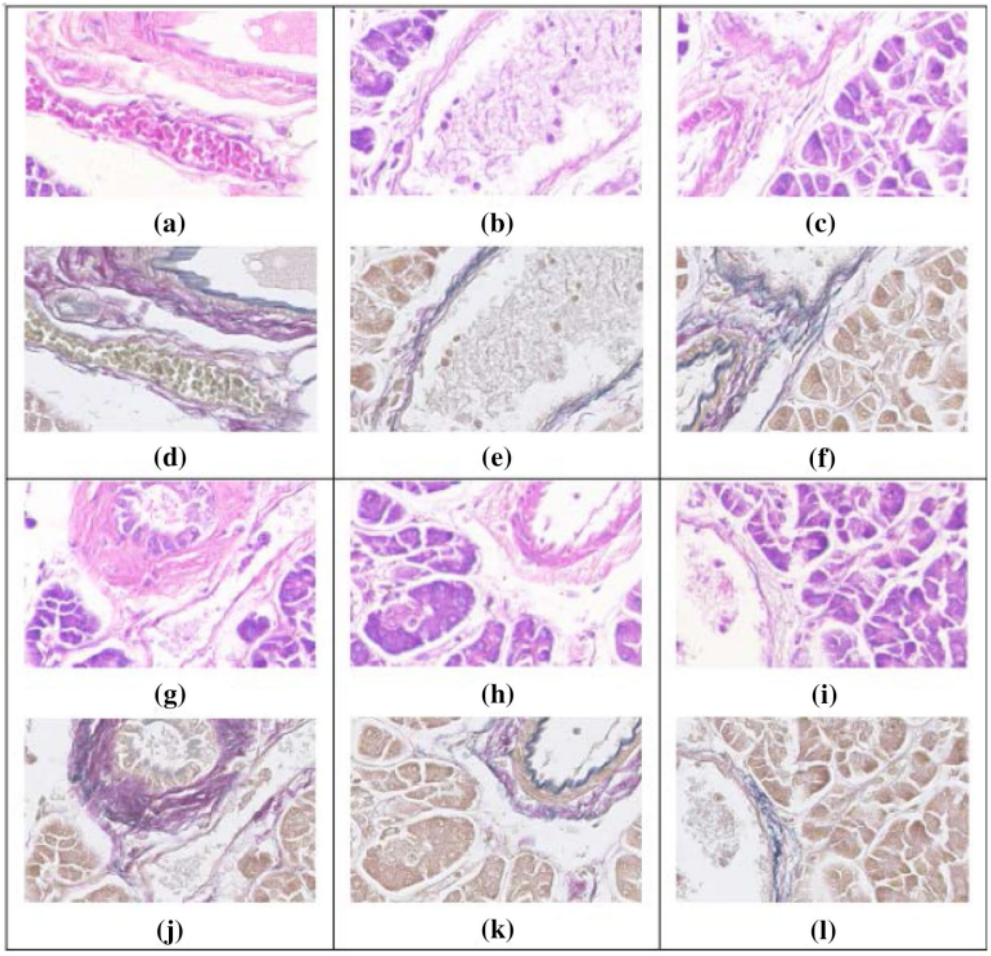

Fig. 6 Image samples, **a–c**, **g–i** H&E stained and **d–f**, **j–l** EVG stained image

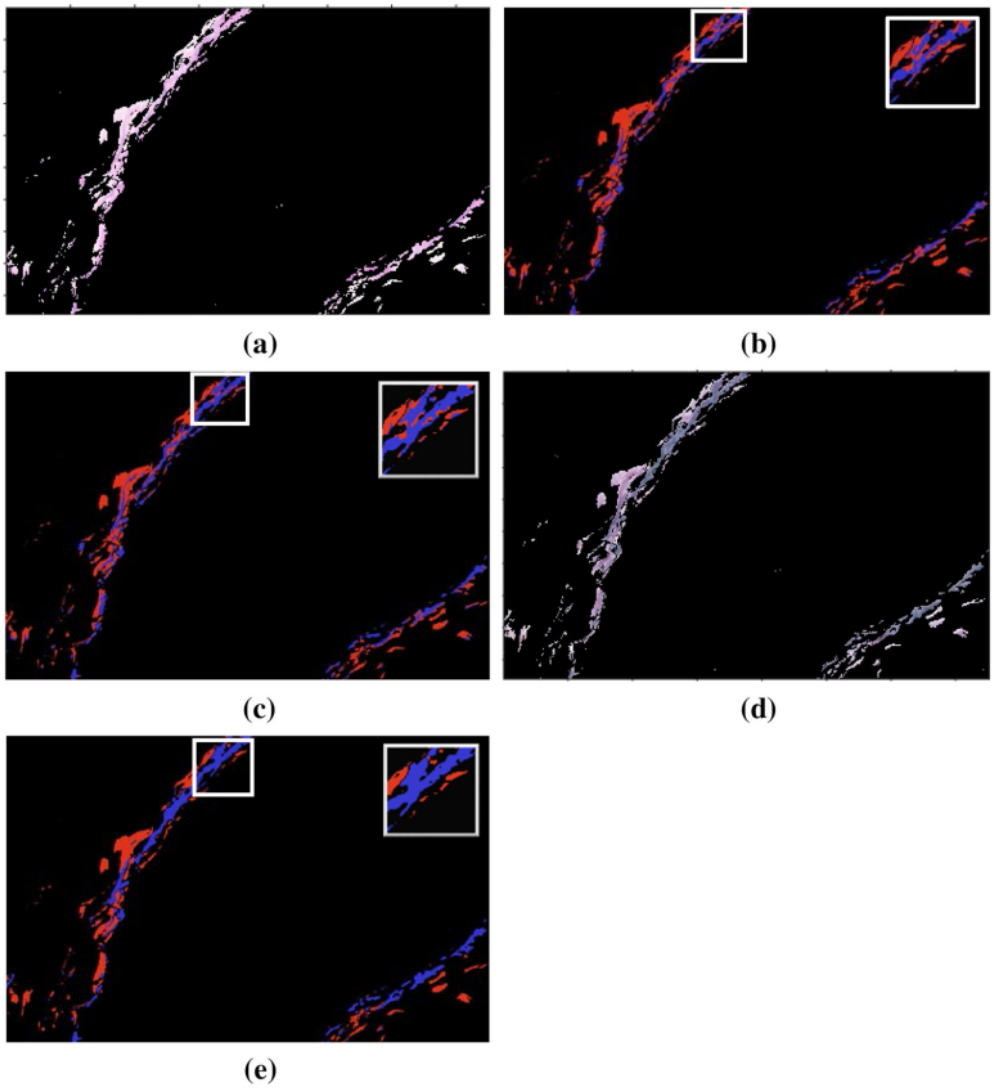

Fig. 7 Resultant images of one cross-validation, **a** fiber region of HE-stained image, **b** classification resultant image from H&E-RGB image, **c** classification resultant image from H&E-hyperspectral image, **d** fiber region of EVG stained image, **e** classification resultant image from EVG image, which is groundtruth of the classification

$$\text{Sensitivity} = \frac{\text{True positive}}{\text{True positive} + \text{False negative}}, \tag{8}$$

$$\text{Specificity} = \frac{\text{True negative}}{\text{True negative} + \text{False positive}}, \tag{9}$$

where true positive and false negative mean the number of pixels where an elastic fiber pixel is decided as elastic fiber correctly and collagen fiber incorrectly, respectively. True negative and false negative also mean the number of pixels where a collagen fiber pixel is decided as collagen fiber correctly and elastic fiber incorrectly, respectively.

With these indexes, we obtained the receiver of curve (ROC) plot of elastic and collagen from each testing image as seen in Fig. 9. These ROC curves were drawn by shifting the decision line for the classification of data projection from minimum to maximum of the score.

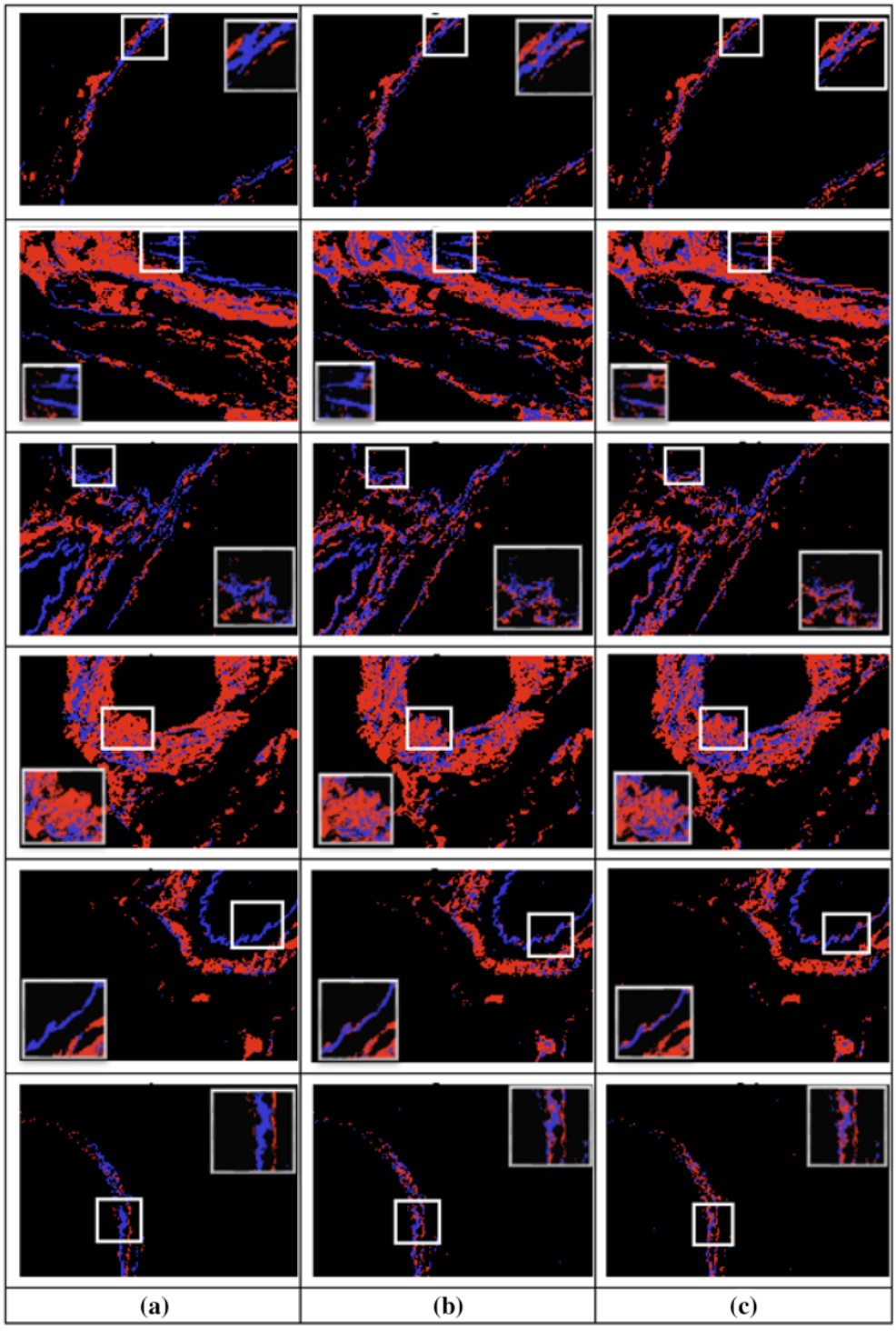

Fig. 8 Resultant image of six cross validations **a** Groundtruths images, **b** resultant images from hyperspectral H&E images, **c** resultant images from RGB H&E images

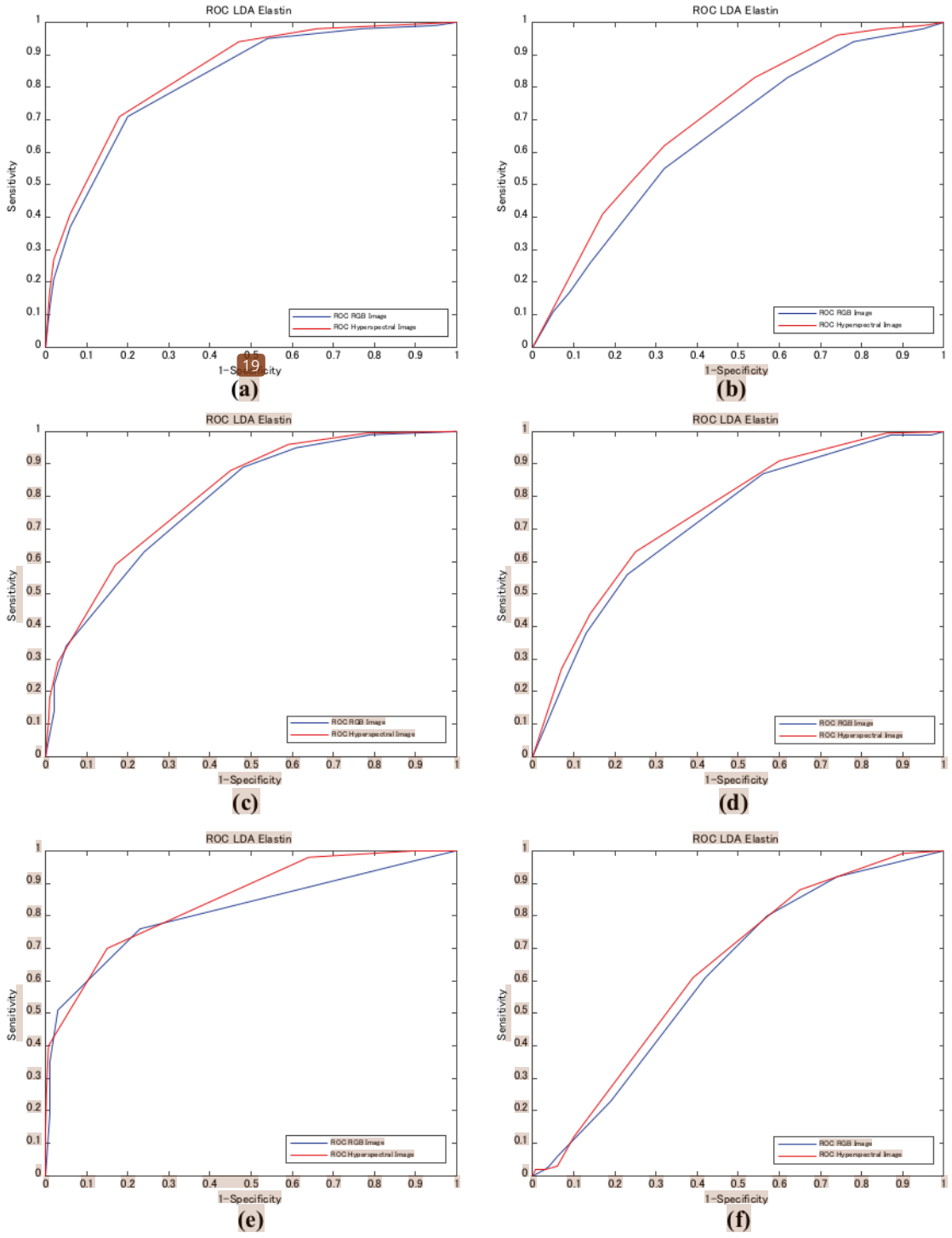

Fig. 9 ROC curves of six cross validations, **a–f** results of cross validation 1–6

Table 1 AUC from six cross validations

Cross validation	Hyperspectral	RGB
1	0.8421	0.8207
2	0.7057	0.6533
3	0.8069	0.7875
4	0.7499	0.7252
5	0.8498	0.8146
6	0.6374	0.6185
Average	0.7653	0.7366
Std.dev.	0.0763	0.0783

To evaluate the accuracy of the classification from the ROC curves, we calculated the area under curve (AUC) as following equation [18],

$$\mathrm{AUC} = \int_0^1 \mathrm{ROC}(t)\mathrm{d}t. \tag{10}$$

The results of AUC are shown in Table 1. This result shows that classification on hyperspectral images performs better than RGB in all samples.

4 Discussion

These observations show that the potential performance of classification based on hyperspectral imaging is superior to classification based on RGB imaging from several points of view. Hyperspectral imaging systems are less cost-efficient compared to RGB camera systems in general. However, a simpler imaging system equivalent to the classification potential based on hyperspectral imaging systems can be realized with a wavelength filter that has a shape of the LDF shown in Fig. 4b.

Meanwhile, this study investigated the classification performance base on only spectral feature information, in which the classification accuracy of the experiment is not good enough to employ the proposed classification method in practical diagnoses. However, the combination of not only spectral but also spatial information can surely improve the classification accuracy. This means that a classification method with sufficient accuracy for practical diagnoses can be realized.

5 Conclusion

This study observed elastic and collagen fibers classification from the H&E-stained image through hyperspectral transmittance using discriminant analysis. The evaluation was done by visual and quantitative verification compared to the classification result of EVG stained image [13], which has been verified by pathologists. The result shows that the hyperspectral result performs better than RGB. It shows the potential method to substitute the usage of EVG staining method to recognize the appearance of elastic fibers.

Acknowledgements This work is supported by Indonesia Endowment Fund for Education (LPDP) and Japan Society for The Promotion of Science (JSPS)—Indonesian Institute of Science (LIPI) Joint Research Program.

References

1. Uitto, J., et al.: Elastin in diseases. J. Invest. Dermatol. **79**, 160s–168s (1982)
2. Lakiotaki, E., et al.: Vascular and Ductal Elastatic Change in Pancreatic Cancer, Acta Pathologica, Microbiologica et Immunologica Scandinavica. Wiley, New York (2015)
3. Piesik, B., Zimmerman, G.: Determination of ocean reflectance by multispectral remote sensing. Acta Astronaut. **11**, 349–351 (1984)
4. Farkas, D., Du, C., Fisher, G., Lau, C., Niu, W., Wachman, E.S., et al.: Noninvasive image acquisition and advance processing in optical bioimaging. Comput. Med. Imaging Graph. **22**, 89–102 (1998)
5. Wilson, B.C., Jacques, S.L.: Optical reflectance and transmittance of tissues: principles and applications. IEEE J. Quantum Electron. **26**, 2186–2198 (1990)
6. Lu, G., et al.: Detection of head and neck cancer in surgical specimens using quantitative hyperspectral imaging. Clin. Cancer Res. **23**(18), 5426–5436 (2017)
7. Bautista, P.A.: Digital staining for multispectral images of pathological tissue specimens based on combined classification of spectral transmittance. Comput. Med. Imaging Graph. **29**, 649–657 (2005)
8. Omucheni, D.L., et al.: Application of principal component analysis to multispectral-multimodal optical image analysis for malaria diagnostics. Malar. J. **13**, 485 (2014)
9. Septiana, L., et al.: Staining Adjustment of Dye Amount to Clarify the Appearance of Fiber, Nuclei, and Cytoplasm in HE-stained Pathological Kidney Tissue Image, International Multidiciplinary Conference and Productivity and Sustainability. Ukrida Press, Jakarta (2017)
10. Abe, T., Murakami, Y., Yamaguchi, M., et al.: Color correction of pathological images based on dye amount quantification. Opt. Rev. **12**, 293 (2005)
11. Yang, T.-Y., Chen. C.C.: Data visualization by PCA, LDA, and ICA. In: The Annual Conference on Engineering and Technology ACEAT-493, 4–6 November (2015)
12. McLachlan, G.J.: Discriminant Analysis and Statistical Pattern Recognition. Wiley Interscience, New York (2004). **(ISBN: 0-471-69115-1)**
13. Abe, T., et al.: Quantification of collagen and elastic fibers using whole slide images of liver biopsy specimens. Pathol. Int. **63**(6), 305–310 (2013)
14. StatSoft, Inc.: Electronic Statistics Textbook. StatSoft, Tulsa (2013). www.statsoft.com/textbook/. Accessed on 30 Nov 2018
15. MathWorks (2018). Statistic and machine learning toolbox: user's guide (R2018b). https://www.mathworks.com/help/pdf_doc/stats/stats.pdf. Retrieved 30 Nov 2018
16. Fisher, R.A.: The use of multiple measurements in taxonomic problems. Ann. Eugen. **7**, 179–188 (1936)

17. Altman, D.G., Bland, J.M.: Diagnostic tests. 1: sensitivity and specificity. BMJ **308**(6943), 1552 (1994). https://doi.org/10.1136/bmj.308.6943.1552. **(PMC 2540489. PMID 8019315)**
18. Jawien, W.: Searching for a n optimal AUC estimation method: a never-ending task. J. Pharmacokinet. Parmacodynamics **41**(6), 655–673 (2014)

Fibers Discriminant

ORIGINALITY REPORT

12%	9%	7%	2%
SIMILARITY INDEX	INTERNET SOURCES	PUBLICATIONS	STUDENT PAPERS

PRIMARY SOURCES

1	www.infona.pl Internet Source	3%
2	sinta3.ristekdikti.go.id Internet Source	2%
3	www.nature.com Internet Source	1%
4	victorwyee.com Internet Source	1%
5	Submitted to School of Business and Management ITB Student Paper	<1%
6	Lu Yan, Masahiro Yamaguchi, Naoki Noro, Yohei Takara, Fuminori Ando. "A novel two-stage deep learning-based small-object detection using hyperspectral images", Optical Review, 2019 Publication	<1%
7	Emrah Tas, Soydan Cakir, Mustafa Cetintas, Pavel Hamouz et al. "Proficiency testing for conducted immunity with a new round robin	<1%

test device", 2016 International Symposium on Electromagnetic Compatibility - EMC EUROPE, 2016
Publication

8	doaj.org Internet Source	<1%
9	Hiroyuki Kobayashi, Qiangfu Zhao. "Face Detection Based on LDA and NN", 2007 Japan-China Joint Workshop on Frontier of Computer Science and Technology (FCST 2007), 2007 Publication	<1%
10	Pinky A. Bautista, Yukako Yagi. "Digital simulation of staining in histopathology multispectral images: enhancement and linear transformation of spectral transmittance", Journal of Biomedical Optics, 2012 Publication	<1%
11	Yuji Odagaki, Masakazu Kinoshita, Toshio Ota, J. Javier Meana, Luis F. Callado, Jesús A. García-Sevilla. "Adenosine A1 receptors are selectively coupled to Gαi-3 in postmortem human brain cortex: Guanosine-5'-O-(3-[35S]thio)triphosphate ([35S]GTPγS) binding/immunoprecipitation study", European Journal of Pharmacology, 2015 Publication	<1%

12	docksci.com Internet Source	<1%
13	royalsocietypublishing.org Internet Source	<1%
14	malariajournal.biomedcentral.com Internet Source	<1%
15	pubmed.ncbi.nlm.nih.gov Internet Source	<1%
16	Yuri Murakami. "Lossless and lossy coding for multispectral image based onsRGB standard and residual components", Journal of Electronic Imaging, 2011 Publication	<1%
17	Bautista, P.A.. "Digital staining for multispectral images of pathological tissue specimens based on combined classification of spectral transmittance", Computerized Medical Imaging and Graphics, 200512 Publication	<1%
18	Liqing Wu, Weiru Fan, Ziyang Chen, Jixiong Pu. "Focusing and polarized modulation of a laser passing through a multi-core fiber", Optical Review, 2019 Publication	<1%
19	"Intelligent Computing Theories and Application", Springer Science and Business	<1%

Media LLC, 2017
Publication

20	en.wikipedia.org Internet Source	<1%
21	Shu Wang, Xiuqiang Chen, Weilin Wu, Zhida Chen, Huiping Du, Xingfu Wang, Yu Vincent Fu, Liwen Hu, Jianxin Chen. "Rapid, label-free identification of cerebellar structures using multiphoton microscopy", Journal of Biophotonics, 2017 Publication	<1%
22	Pinky A. Bautista, Noriaki Hashimoto, Yukako Yagi. "Color standardization in whole slide imaging using a color calibration slide", Journal of Pathology Informatics, 2014 Publication	<1%
23	Pinky A. Bautista, Yukako Yagi. "Staining Correction in Digital Pathology by Utilizing a Dye Amount Table", Journal of Digital Imaging, 2015 Publication	<1%

Exclude quotes	On	Exclude matches	Off
Exclude bibliography	On		